

Phase transformation and precipitation hardening behavior of Cr and Fe in BS40CrFeSn alloy

Shufeng Li · Hisashi Imai · Haruhiko Atsumi ·
Katsuyoshi Kondoh

Received: 16 March 2010/Accepted: 17 May 2010/Published online: 3 June 2010
© Springer Science+Business Media, LLC 2010

Abstract Phase transformation and precipitation hardening behavior of the water atomized copper alloy powder was studied by aging treatment, to develop high strength Cu–40Zn–X (X: Cr, Fe, Sn) alloys by powder metallurgy process. Super-saturated solid solution elements of Cr and Fe are formed in the brass matrix, and single β phase was retained in the raw powder after water atomization. Solid solubility of Cr and Fe decreased with increase of aging temperature, and phase transformation evolved from single β phase to $\alpha + \beta$ duplex phase structure after aged at the elevated temperature of 773 K and over. It was clarified that Cr showed higher precipitation potential than Fe in the brass matrix. The hardness depended strongly upon solid solubility of Cr and Fe, and upon phase transformation.

Introduction

Widely used $\alpha + \beta$ duplex phase brasses have the best combination of high technological and service properties. In recent years, the impetus for the development of lead-free brasses and the development of the electronics industry has led to a number of new applications for brasses including lead frames, connectors, and other electronic components [1, 2]. These applications require brasses with unique combinations of mechanical strength and conductivity coupled with environment amiability.

Several factors should be carefully considered in designing high strength copper alloys, these factors are: (1)

effective precipitation strength, (2) little adverse effect on machinability and conductivity, (3) simple and cost-effective manufacturing process, and (4) inexpensive and non-toxic alloying elements. The binary phase diagrams of copper alloys [3] indicate that Cr, Fe, Ti, P, Co, Mg, Sn, etc. could serve as candidate alloying elements for precipitation strengthening high strength and high conductivity copper alloys, because the solid solubility of these alloying elements would decrease sharply with the decreasing temperature in copper. However, the strength of binary alloys is limited, in order to obtain higher strength, more than one alloying elements are needed to form intermetallic precipitates, such as CrFe [4], Fe₂P [5], FeTi and Cu₄Ti [6], Cu₃Zr [7], etc. during aging process.

Cu–Cr alloys have a large precipitation hardening response, this is because the super-saturation of Cr in the Cu matrix creates a high degree of thermodynamic metastability in the solution-treated condition, thus providing a high chemical potential for the precipitation reaction of Cr [8, 9]. For commercial Cu–Fe alloys, Fe rich precipitates serve to stabilize the cold worked microstructure. Cu–Fe alloys also have the advantage of being easier to process than Cu–Cr. Fernee et al. [8] reported additional strength is provided by iron, a grain refiner that is virtually insoluble in α and β phases and appears as precipitates of an iron-rich intermetallic compound.

Very few reports available, which give detailed information on the influence of Cr and Fe to phase transformation and mechanical properties of $\alpha + \beta$ duplex phase brasses by powder metallurgy methods, which is worthy of investigation. In powder metallurgy, it is possible to fabricate components which otherwise would decompose or disintegrate in direct alloying of melted materials. Powder processes are more flexible than casting and forging techniques, it is used in a wide range of industries, from

S. Li (✉) · H. Imai · H. Atsumi · K. Kondoh
Department of Composites Processing, Joining and Welding
Research Institute, Osaka University, 11-1, Mihogaoka, Ibaraki,
Osaka 567-0047, Japan
e-mail: shufengli@hotmail.com

automotive and aerospace applications to power tools and household appliances.

The strengthening effect in conventional solid solution aging is limited due to low solubility of Cr and Fe in Cu with coarse grain structure at the solid solution temperature. Rapid solidification, e.g., high cooling rate can lead to super-saturated solid solution of Cr and Fe in Cu matrix. Upon aging very fine dispersoids of second phase are precipitated in the matrix, as a result, the precipitation hardening effect is greatly intensified. The purpose of the present investigations was to develop a high strength brass, combined the properties of precipitation hardening response of chrome and iron additions. The effects of the aging temperature on precipitation behavior, phase transformation and solute diffusions, and resulted mechanical properties were investigated in detail.

Experimental

The Cu–40 wt%Zn–0.98Cr–0.63Fe0.65Sn (denoted as BS40CrFeSn) composition was selected as experimental alloy at present research. Cr and Fe are chosen for their abilities to form Cr–Fe co-precipitates, or either as separate phases during aging process. Moreover, the effect of Fe and Cr upon each other's solid solubility in the brass matrix was unknown, but appeared to be worth investigating. A Cr content of 0.98% was selected based upon the maximum equilibrium solubility of Cr in Cu is about 0.8 wt% at 1,343 K [10], and a slight excess of Cr was chosen to compensate the consumption of Cr in the formation of CrFe intermetallic compound (σ), which is predicted according to the Fe–Cr equilibrium phase diagram. The maximum practical solubility of Fe in Cu is 2.5 wt% [3]. For this reason, the addition of 0.65% Fe in experimental alloy was selected, because the effect of 0.98 wt% Cr and 40 wt% Zn upon the solid solubility of Fe in Cu matrix unknown. The addition of 0.6 wt% Sn was selected to improve corrosion resistance and somewhat higher strength, moreover, Sn was added to reduce susceptibility to dezincification.

BS40CrFeSn copper alloy was prepared in this experiment, for which the nominal composition (wt%) was 0.98Cr, 0.63Fe, 0.65Sn, and 40.4Zn, with the balance being Cu. The alloy was melt in an electrical induction furnace with an argon atmosphere and kept at 1,673 K for several minutes to make the melt homogeneous. The molten alloy was poured into a heated tundish at 1,673 K. In the water atomization process, high pressure water jets were directed against the molten stream to prepare rapidly solidified BS40CrFeSn alloy powder. The atomized powders were collected, dried, and sieved. The chemical compositions and particle size analysis were carried out, and the results

Table 1 Chemical composition of the as-atomized BS40CrFeSn powder

| Powders | Particle size (μm) | | Mass% | | | | | |
|------------|------------------------------------|--------------|-------|------|-------|-------|-------|------|
| | Median size | Mean size | Zn | Cr | Fe | Sn | O | Cu |
| BS40CrFeSn | 184.3 | 206.8 | 40.5 | 0.98 | 0.629 | 0.648 | 0.083 | Bal. |

are shown in Table 1. Thermal analysis system (DTG-60/60H, Shimadzu) was employed with a combination of thermogravimetry (TG) and differential thermal analysis (DTA) to investigate the physic properties of the as-atomized powder.

As-atomized BS40CrFeSn alloy powder was used as raw material, with a mean particle size of 206.8 μm . 100 g alloy powder was pressed with a pressure of 600 MPa by a hydraulic press machine. The billets obtained with the diameter of 11 mm, were heat treated at 773, 873, and 1,053 K, respectively, with a muffle furnace (KDF, S-70 Denken) in nitrogen gas atmosphere. After kept for 1.8 ks, the power was shut down and the sample was cooled inside the furnace below than 323 K. The schematic sketch of the water atomized powder procedure and heat treatment of the samples are shown in Fig. 1.

The phase compositions in samples were identified by using X-ray diffraction (Labx, XRD-6100, Shimadzu) referenced to the standard ICDD PDF cards available in the system software. The micro-hardness was measured by Vickers micro-hardness tester (HMV-2T, Shimadzu), 10 measurements were conducted to obtain an average value. In addition, the microstructure evolution of the raw powder and samples were conducted by using field-emission scan electronic microscope (FE-SEM, JEM-6500F, JEOL), phases were examined by the energy-dispersive X-ray spectrometer (EDS) equipped by the SEM.

Results and discussion

As-atomized powder's characteristics

The FE-SEM micrographs of the raw powder are depicted in Fig. 2. The particle shows an irregular shape with a mean particle size of 206.8 μm (Fig. 2a). The observation at higher magnification of the cross section confirmed the grain size of 0.5–2 μm (Fig. 2b).

Figure 3 shows the XRD diffractography of the as-atomized powder. It can be observed that the raw powder showing predominantly β phase peak, the analysis result is agreeable with the status that the raw powder was produced by rapid solidification method, rapid cooling from the β phase field retains a single β phase state in the powder.

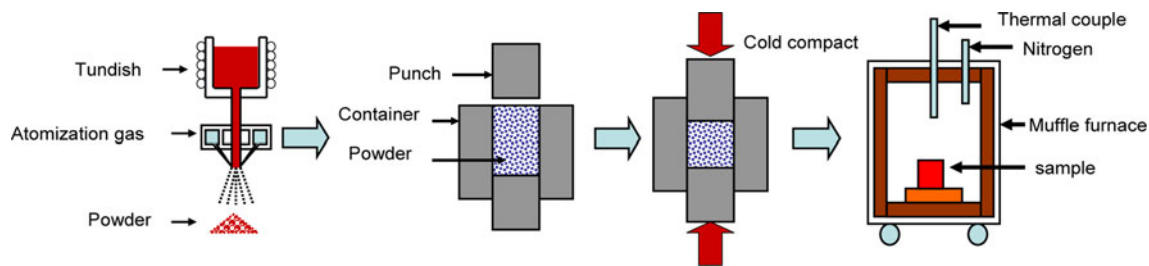


Fig. 1 Schematic sketch of the water atomize powder procedure and the sample heat-treatment process

Fig. 2 FE-SEM microstructure of the water atomized CuZn alloy powder. **a** As-produced powder and **b** cross section of the raw powder

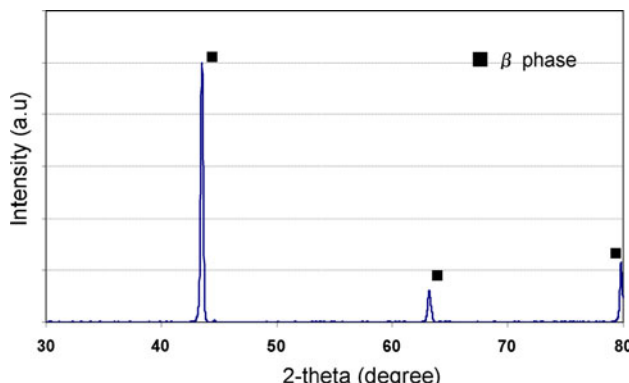
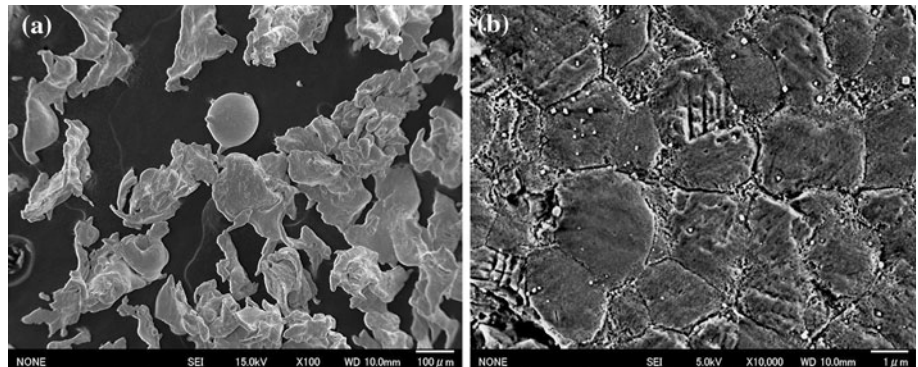


Fig. 3 X-ray diffractography of the BS40CrFeSn raw powder

The DTA and TG of the powder were carried out and the results are shown in Fig. 4. An endothermic peak can be observed at 726 K, which suggests phase transformation of β' to β happened, referring to the Cu–Zn binary phase diagram. Zn began to vaporize at 982 K, 42.9 wt% mass was lost when the temperature increase to 1,273 K, which indicates nearly all the Zn vaporized at 1,273 K. No obvious endothermic peak can be observed at temperature <726 K, which means the phase transformation of β to α was slow and successive at low heating rate of 283 K/min.

Phase transformations

The X-ray diffractography of the BS40CrFeSn alloy after aged at different temperature are shown in Fig. 5. In the

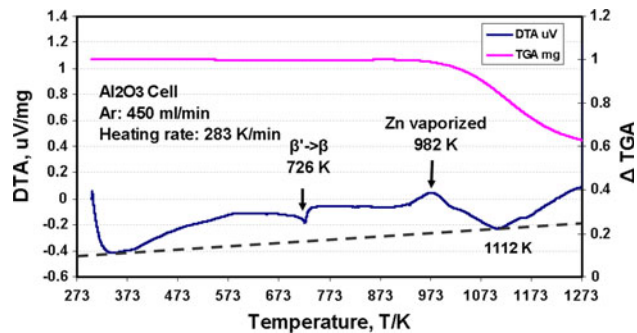


Fig. 4 The differential thermal analysis (DTA) and thermogravimetry (TG) of the as-produced powder was analyzed from 283 to 1,273 K, heating rate is 283 K/min, the powder was protected by argon at 450 mL/min

green compact, tiny α phase peak appeared at 42.324°, indicates recrystallization happened and parts of β phase transformed into α phase after subjected to 600 MPa pressure in the preparation of the green compact. Furthermore, the peak appeared at 44.548° in the green compact represented the existence of Cr1.36Fe0.52 intermetallic compound (IMC), which implied the IMC derived from the process of powder preparation. Moreover, the intensity of Cr1.36Fe0.52 IMC showed nearly no variation with the elevated aging temperatures, indicating Cr1.36Fe0.52 IMC was stable even experiencing high temperatures. The main peak of zinc oxide (ZnO) appeared at 36.495°, indicating zinc vaporized and oxidized at 773 K, and getting severe at elevated temperature. Furthermore, the Cr peak can be

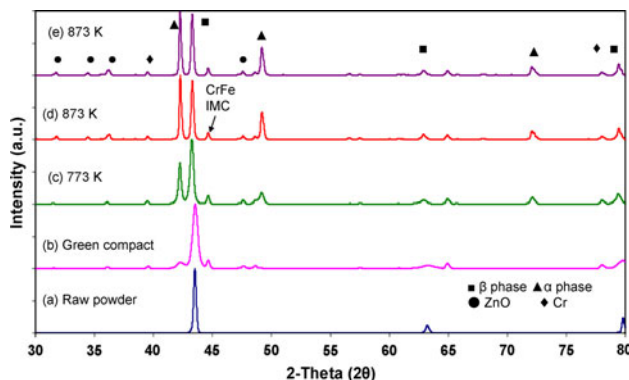


Fig. 5 The X-ray diffractography of the BS40CrFeSn alloy before and after aging at different temperatures

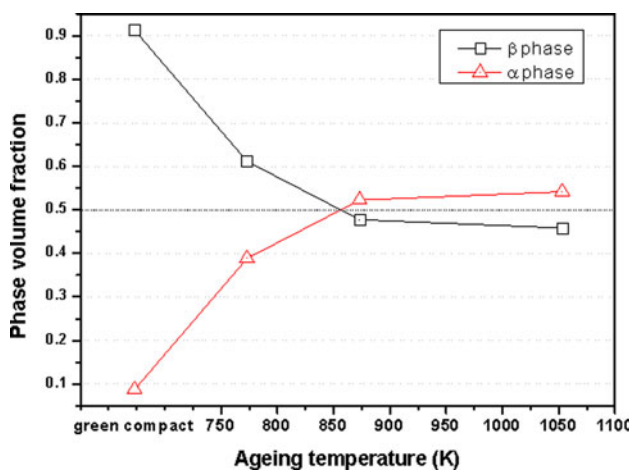


Fig. 6 Phases volume fractions versus different aging temperatures calculated by the diffraction peak intensity

observed at different temperature, showing solid soluted Cr element precipitated and pure Cr existed in the samples.

The quantitative analysis of different phases in the samples can be calculated by the diffraction peak intensity [11]. The α phase volume fraction shows an increase trend at elevated temperature from 773 to 1,053 K, increasing from 8.75% in green compact to 54.16% at 1,053 K, as shown in Fig. 6. The ratio of α phase versus β phase close to 1, indicates the volume fraction of α and β phases is equal when the aging temperature higher than 873 K. The increase of α phase with elevated temperature are considered due to Zn vaporization at high temperature. The volume fraction of CrFe IMC is ignored for its minor content at the present calculations.

Microstructures

The microstructures of the samples before and after aging are shown in Fig. 7. Raw powder is mainly β phase and includes ultrafine dispersoids distributing uniformly in

brass matrix (Fig. 7a). After aging at 773 K for 1.8 ks, recrystallized α phase with network structure existed at the β phase grain boundaries. At the same time, the ultra-fine particles distributed uniformly and grew coarser (Fig. 7b). α phase grew rapidly and became coarser, constrained Cr and Fe in the super-saturated solid powder precipitated and the dispersoids grew coarser after aged at 873 K (Fig. 7c). When the sample was heated at 1,053 K for 1.8 ks, the grains of α and β phases grew rapidly and became coarser. The dispersoids also became coarser and the population decreased sharply (Fig. 7d).

The compositions of the phases and compounds in the samples were analyzed by EDS. In the sample aged at 1,053 K as shown in Fig. 8. The coarser dispersoids distributed inside grains, EDS result indicates that the particles were Fe rich metastable dispersoids, including 53.38 wt% of Fe, 22.5 wt% of Cr as shown in Table 2. It can be found fine Cr particles precipitated at the triple junction of primary particle boundaries. The coarse CrFe IMC embedded in the matrix can be observed, the composition of the CrFe IMC is 71.34 wt% Cr and 22.38 wt% Fe, which is in good agreement with the XRD analysis result indicating the existence of Cr1.36Fe0.52 IMC at 44.548° as shown in Fig. 5. In order to confirm the origin of the CrFe IMC, cast ingot was prepared with equivalent composition as that of as-atomized powder, which was shown in Fig. 9. The large CrFe IMC dentrite can be observed in the cast ingot as shown in Fig. 9a, CrFe IMC nucleated and grew large when the melting alloy was cooled. During water atomization process, CrFe IMC was nucleated but has inadequate time to grow into dentrite with rapid solidification, which was remained inside powder particles and shown a different morphology as revealed in Fig. 9b.

Solid solubility and micro-hardness

The solid solubility of Cr and Fe in brass matrix are shown in Fig. 10a, which decreased with the increase of aging temperatures both in α and β phases. The solid solubility of Cr and Fe in green compact are 0.89 and 0.78 wt%, respectively, decreased to 0.26 and 0.19 wt% after aged at 1,053 K for 1.8 ks. The compositions of Cr and Fe in IMC show nearly no varieties with the increase of aging temperature as shown in Fig. 10b, illustrating the CrFe IMC is stable and do not change at elevated aging temperatures.

The effect of aging temperature on Vickers micro-hardness of the matrix and IMC are shown in Fig. 11a. The Vickers micro-hardness decreased rapidly from 203 to 102 Hv when the aging temperature increased to 1,053 K. However, the micro-hardness of IMC showed nearly no variation with the elevated aging temperature. The relationship between solid solubility of Cr and Fe in brass

Fig. 7 Microstructure of BS40CrFeSn alloy before and after aging at different temperatures for 1.8 ks. **a** Green compact, **b** 773 K, **c** 873 K, and **d** 1,053 K

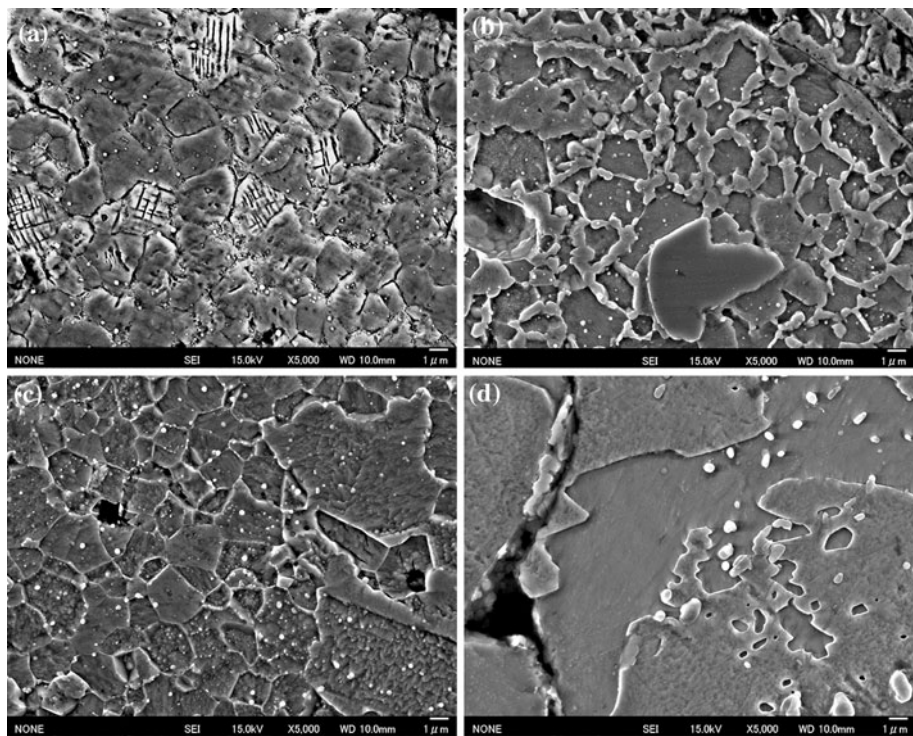


Fig. 8 The SEM micrography of the sample after aged at 1,053 K and the EDS mapping analysis

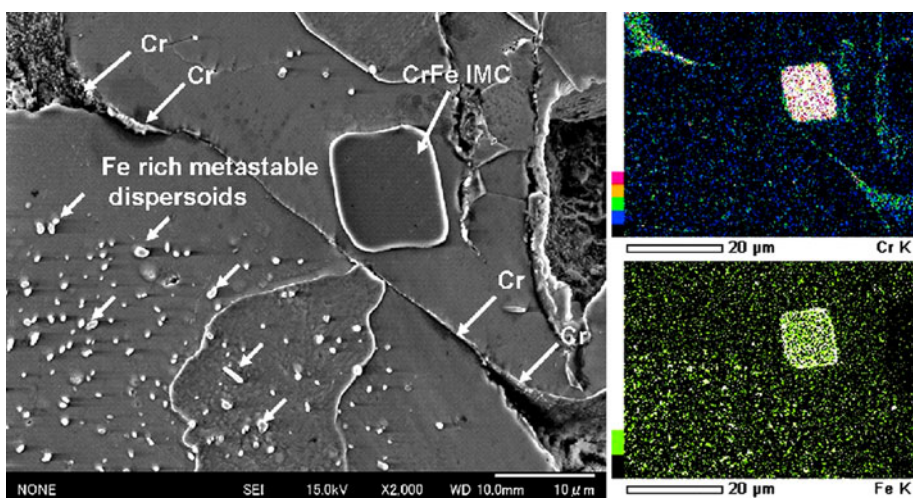


Table 2 Chemical composition of the dispersoids in the sample of aging at 1,053 K by EDS analysis

| Dispersoids | Chemical composition, mass% | | | | |
|---------------------|-----------------------------|-------|-------|------|-------|
| | Zn | Cr | Fe | Sn | Cu |
| CrFe IMC | 2.86 | 71.34 | 22.38 | 0.09 | 3.32 |
| Fe rich dispersoids | 10.30 | 22.50 | 53.38 | 0.26 | 13.57 |

matrix and Vickers micro-hardness are shown in Fig. 11b. It can be observed that the solid solubility of Cr and Fe decrease with increase of the aging temperature, Vickers micro-hardness showed nearly similar decrease trend, which implied the hardness of the matrix dependent

heavily upon the solid solubility of Cr and Fe. On the other hand, the β phase volume fraction decrease is another effective factor on the matrix hardness.

Discussion

The maximum equilibrium solubility of Cr in Cu is 0.8 wt% at 1,343 K [10]. The maximum solubility of Fe in Cu is 4.1 wt% [3], however, the solubility of Cr and Fe in Cu decrease rapidly as the temperature drops according to the phase diagram. At present study, BS40CrFeSn alloy powder was prepared by water atomized method with rapid

Fig. 9 The SEM micrography of the morphologies of CrFe intermetallic compound. **a** Cast ingot sample and **b** cross section of the as-atomized powder

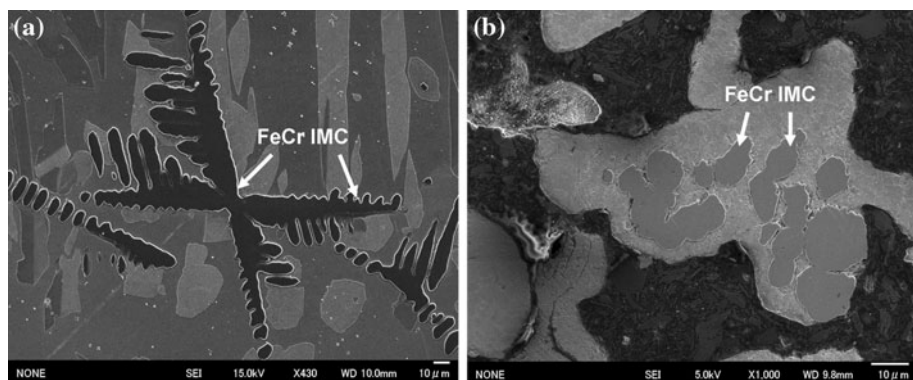


Fig. 10 Solid solubility of Cr and Fe as a function of aging temperatures. **(a)** Solid solubility of Cr and Fe in α and β phases and **b** contents of Cr and Fe in CrFe IMC

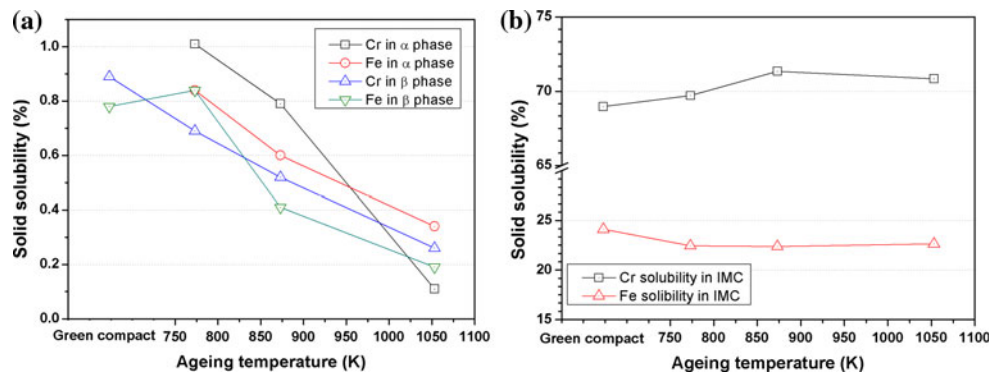
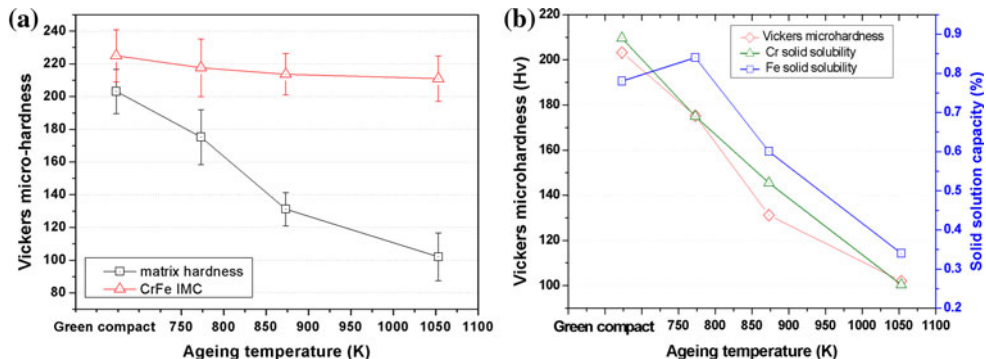


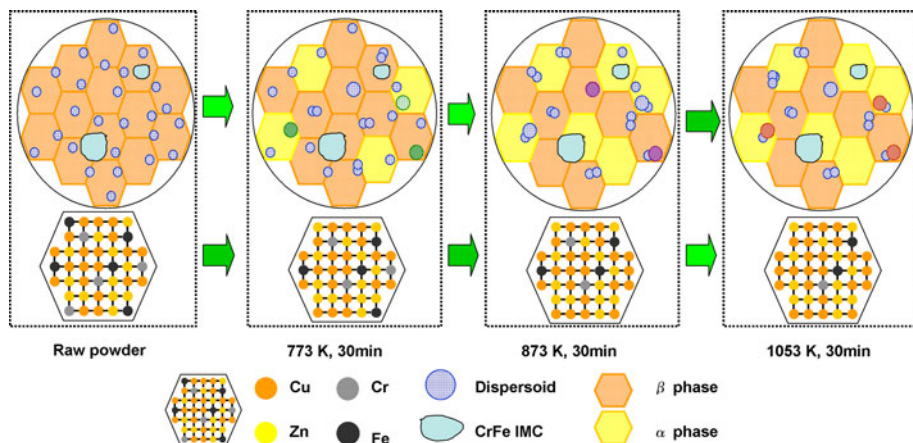
Fig. 11 Vickers micro-hardness of the matrix and IMC as a function of aging temperature (a), and the effect of solid solubility of Cr and Fe on Vickers micro-hardness at different aging temperatures (b)



solidification. A high cooling rate can lead to the formation of a more refined microstructure and extended solid solubility and even metastable phases [12, 13]. Thus, the super-saturated solid solutions of Cr and Fe in brass are formed. The solid solubility of Cr and Fe in brass matrix are 0.89 and 0.78 wt% in the raw powder at room temperature, respectively. The difference in atomic radius between these alloying elements provides a strain field, which is beneficial to the solid solution strength. However, the solid solubility of Cr and Fe decrease rapidly with the elevated aging temperature, deteriorating the mechanical properties. On the other hand, it can be observed fine dispersoids dispersed on the brass matrix. The Fe–Cr equilibrium phase diagram [3] shows that Fe and Cr have complete solid solubility in one another at elevated temperature. Cr atoms are similar in size to Fe atoms, the bond length for Cr and

Fe pure metals in their bcc phase are 0.24980 and 0.24832 nm, respectively [14]. Therefore, when Cr is alloyed in Fe at a level of not more than 11 wt% Cr, the Cr atoms replace some of the Fe atoms, thus forming a substitutional solid solution [2]. Chrome addition has a large precipitation hardening response in copper, because of the super-saturation of chrome in the copper matrix creates a high degree of thermodynamic meta-stability, thus providing a high chemical potential for the precipitation reaction of chrome [8]. As a result, after aged at elevated temperature, these dispersoids coalesced and grew coarser, and Cr precipitated at the primary particle boundaries. However, Fe was remained inside the dispersoids. The procedures of the precipitation behavior and phase transformation at elevated aging temperature are schematic illustrated in Fig. 12.

Fig. 12 Schematic sketches of the procedure of phase transformation and solid solution at elevated aging temperature



The super-saturated solid solution of Cr and Fe resulted in the solid solution strength, which is beneficial to the hardness. Furthermore, precipitate strengthening derived from the fine dispersoids also profits the mechanical strength. In solid mechanics, the material hardness is described as the resistance to deformation in crystalline solids, which is inherently size dependent over a scale that range from a fraction of micron to a hundred microns or so, with smaller being harder [15]. One source of this size dependence is that internal obstacles, such as incoherent precipitates and grain and phase boundaries, restrict glide, leading to dislocation pile-ups that further restrict dislocation motion. As a consequence, the mechanical properties increase as the scale of microstructure decrease.

Conclusions

BS40CrFeSn powder was prepared by water atomized method with high cooling rate, and the characteristics of the powder, phase transformation and precipitation behavior at elevated aging temperature were investigated.

- (1) β phase was retained in the powder by water atomized method. Phase transformation took place after heated at 773 K. The volume fraction of α phase increased and is equal to that of β phase when the aging temperature higher than 873 K.
- (2) The solid solubility of Cr and Fe in brass matrix decreased with elevated aging temperature, combined with the phase transformation from β to α phases, which affected the matrix hardness remarkably.
- (3) Cr showed higher precipitate potential than Fe in Cu–40ZnCrFeSn rapidly solidified alloy matrix.

Acknowledgments This work was financially supported by Regional Research and Development Resources Utilization Program, Japan Science and Technology Agency (JST). The authors extend their thanks to Nihon atomized metal powders corporation (Project Manager: Mr. Koji Yamamoto, Mr. Motoi Takahashi, and Mr. Eisuke Yotsuka), for providing powders used in this study. And also grateful to San-Etsu metals Co. LTD. (Project Manager: Mr. Yoshiharu Kosaka and Mr. Akimichi Kojima), for their technical supports in this study. The authors sincerely thank the researchers of the Joining and Welding Research Institute (JWRI) in Osaka University, Mr. Yoshi-nori Muraki, Ms. Sachio Nakamura, and Mr. Kyugo Inui for assistant carrying out extrusion experiment.

References

1. ASM (1984) Metals handbook, Desk edition. ASM, OH, p 71
2. Davis JR (2001) Alloying, understanding the basics. ASM International, Materials Park
3. ASM (1990) Metals handbook, alloy phase diagrams, ASM handbook, vol 3, 10th edn. ASM, OH
4. Fernee H, Nairn J, Artens A (2001) J Mater Sci 36:5497. doi: [10.1023/A:1012414605163](https://doi.org/10.1023/A:1012414605163)
5. Lu D-p, Wang J, Zeng W-j, Liu Y, Lu L, Sun B-d (2006) Mater Sci Eng A 421:254
6. Vaidyanathan TK, Mukherjee K (1976) Mater Sci Eng 24:143
7. Liu P, Su J, Dong Q, Li H (2005) J Mater Sci Technol 21:475
8. Fernee H, Nairn J, Artens A (2001) J Mater Sci 36:2711. doi: [10.1023/A:1017916930459](https://doi.org/10.1023/A:1017916930459)
9. Artens A, Nairn J, Fernee H, Skennerton G, Olofinjana A (1997) Mater Forum 21:57
10. Tenwick MJ, Davies HA (1988) Mater Sci Technol 98:543
11. Chu G, Cong YF, You HJ (2003) Acta Metall Sin 166:489
12. Jones H (1996) Mater Lett 26:133
13. Katgerman L, Dom F (2004) Mater Sci Eng A 375–377:1212
14. Weast RC (ed) (1965) Handbook of chemistry and physics, 46th edn. Chemistry and physics. CRC Press, Boca Raton, p 119
15. Zhang LY, Jiang YH, Ma Z, Shan SF, Jia YZ, Fan CZ, Wang WK (2008) J Mater Proc Technol 207:107